18th International Conference on Information Fusion
Washington, DC - July 6-9, 2015

Context-Based Ground Target Tracking - An Integrated Approach

Michael Mertens
Sensor Data and Information Fusion
Fraunhofer FKIE
Wachtberg, Germany
michael.mertens@fkie.fraunhofer.de

Martin Ulmke
Sensor Data and Information Fusion
Fraunhofer FKIE
Wachtberg, Germany
martin.ulmke@fkie.fraunhofer.de

***Abstract*—The general focus of this paper is the improvement of state-of-the-art Bayesian tracking filters specialized to the domain of ground moving objects to obtain high-quality track information, based on airborne ground moving target indication (GMTI) radar measurements. To counteract the numerous challenges, in particular, imprecise measurements and missed detections, a strong false alarm background, closely-spaced targets, technical and terrain obscuration as well as complex target motion, it is highly advisable to exploit additional context information in a tracking system. Three different classes of information are considered and used as extensions of standard tracking algorithms. These are the knowledge on range and Doppler blind zones of the GMTI sensor, road network information and signal strength measurements, where the latter is used to obtain estimates of a target's mean radar cross section (RCS). The performance of differently augmented cardinalized probability hypothesis density (CPHD) filter variants is assessed based on a multi-target simulation scenario.**

Keywords: Bayesian target tracking, ground moving target indication (GMTI), context information, blind zone, road network, signal strength, radar cross section (RCS).

I. Introduction

Tracks of moving objects serve as an essential building block for the detailed situation picture production of a generally complex and dynamically evolving scenario with a wide range of applications. The present work focuses on ground moving targets observed by airborne GMTI radar which is the sensor of choice in this context due to its wide-area surveillance, day & night operation and real-time processing capabilities. The obtained track information then provides essential support for human decision makers or decision making systems. The further developments and enhancements discussed in this paper aim at improving the quality of the track output in the presence of the aforementioned challenges.

The incorporation of context knowledge into the Bayesian filtering scheme has been studied by the authors in detail for several sources of information. Relevant contributions on signal strength information processing are discussed in [1]–[3], where the mean RCS of a target is estimated based on fluctuating signal strength measurements. Exploiting extended knowledge on Doppler and range blind zones of the GMTI sensor is treated in [4], [5] and roads and road networks are focused on in [1], [6]. In comparison with these previous publications, the novelty of the present work is the *combined* processing of these sources of information within the CPHD filter [7], yielding the integrated CPHD filter variant, and its performance evaluation based on a challenging simulation scenario.

The paper is organized as follows: Section II presents the tracking algorithm exploiting context information. In the first part, Section II-A, the standard CPHD filter is briefly reviewed. After that, the three different sources of information used in this paper are briefly discussed and relevant equations given in Section II-B. And in the third part, Section II-C, the integrated variant of the CPHD filter is presented. Section III contains the performance analysis of the developed CPHD filter variants based on a simulation scenario. Finally, concluding remarks are given in Section IV.

II. Target Tracking with Context Information

A. Standard CPHD Filter

The CPHD filter is a recursive Bayesian [8] multi-target estimation scheme based on finite set statistics (FISST) [9] and was first published in [7]. Its main idea is to represent a multi-target state at time t_k by a random finite set (RFS) Ξ_k, where both the elements as well as the number of elements of the set are random variables. In addition, also the measurement sequence $\mathcal{Z}^k = \{Z_1, Z_2, ..., Z_k\}$ with $Z_k = \{\mathbf{z}_k^m\}_{m=1}^{m_k}$ is represented as an RFS. The CPHD sequentially estimates the first-order statistical moment of the full multi-target probability density function (pdf), denoted by $v(\mathbf{x}_k)$. It is called probability hypothesis density (PHD) or intensity function. Within a Gaussian framework [10] with linear motion and measurement models, it is given by a weighted sum of Gaussians as

$$v(\mathbf{x}_k) = \sum_{n=1}^{N_k} w_k^n \, \mathcal{N}(\mathbf{x}_k; \mathbf{x}_k^n, \mathbf{P}_k^n) \ , \qquad (1)$$

where w_k^n, $\mathbf{x}_k^n$ and $\mathbf{P}_k^n$ are the weight, mean and covariance of the Gaussian component n. $v(\mathbf{x}_k)$ corresponds to the probability of having a target in an elementary volume of the state space. Thus, the integral of this function over the state space yields the estimated number of targets. The CPHD filter sequentially computes the cardinality distribution $p(n_k)$ along with $v(\mathbf{x}_k)$, so that the estimated number of targets can also be obtained by $\hat{n}_k = \sum_{n_k=1}^{\infty} n_k\, p(n_k)$. Based on estimates of the intensity function at time step t_{k-1}, the target motion model is employed in the prediction step to obtain first estimates for time step t_k, $v_{k|k-1}(\mathbf{x}_k)$, based on the Kalman prediction equations [8]. And the cardinality distribution is predicted by making use of predefined survival and target appearance probabilities, as described in [7], [11]. In the filtering step at time instance t_k, utilizing all measurements up to t_k denoted by subscript $(k|k)$, the intensity function and the cardinality distribution are updated by

$$v_{k|k}(\mathbf{x}_k) = \left[P_d \frac{\mathcal{L}(\mathbf{Z}_k|D)}{\mathcal{L}(\mathbf{Z}_k)} + (1-P_d)\frac{\mathcal{L}(\mathbf{Z}_k|\neg D)}{\mathcal{L}(\mathbf{Z}_k)} \right] v_{k|k-1}(\mathbf{x}_k) \quad (2)$$

$$p_{k|k}(n_k) = \frac{\mathcal{L}(\mathbf{Z}_k|n_k)}{\mathcal{L}(\mathbf{Z}_k)} p_{k|k-1}(n_k) \quad , \quad (3)$$

where P_d denotes the detection probability and the expressions $\mathcal{L}(\cdot)$ are likelihood ratios as given in, e.g., [11], [12]. All likelihood ratios depend on the weighted single-target detection likelihood L_k^m determined by

$$L_k^m = \frac{1}{n_{k|k-1}} \int P_d\, v_{k|k-1}(\mathbf{x}_k)\, l(\mathbf{z}_k^m|\mathbf{x}_k)\, d\mathbf{x}_k \quad . \quad (4)$$

Under the linear Gaussian measurement model assumption, i.e., $\mathbf{z}_k^m = \mathbf{H}_k \mathbf{x}_k + \mathbf{w}_k^m$ with measurement matrix $\mathbf{H}_k$, Gaussian measurement error $\mathbf{w}_k^m$ and covariance $\mathbf{R}_k^m$, the single-target detection likelihood $l(\mathbf{z}_k^m|\mathbf{x}_k)$ can be written as a Gaussian with $\mathcal{N}(\mathbf{z}_k^m; \mathbf{H}_k\, \mathbf{x}_k, \mathbf{R}_k^m)$ and the Gaussian mixture framework is conserved under the measurement update.

B. Tracking Filter Extensions

In the following, the considered classes of context information are briefly summarized, stating the main ideas and relevant equations based on a general Bayesian filtering scheme.

1) Doppler and Range Blind Zones: The radial velocity component of a moving object induces a measurable phase shift from pulse to pulse in the back-scattered signal. Whenever this range-rate equals a multiple of the sensor's blind speed $\dot{r}_B = \lambda/2\, f_{PRF}$, i.e., $\pm i\, \dot{r}_B$ with $j = 0, 1, 2, \ldots$ and the radar center wavelength λ, then the associated reflection is treated as clutter echo and is therefore suppressed. In that way, multiple Doppler blind zones arise where the width is determined by the width of the space-time adaptive processing (STAP) clutter filter [13], [14]. In addition, as a monostatic radar system permanently switches between transmit and receive mode, dead zones in time occur during which the radar is blind, i.e., no reflections can be received. These time intervals correspond to certain distances, namely multiples of the unambiguous range $R_u = c/(2\, f_{PRF})$, i.e., $j\, R_u$ with $j = 1, 2, \ldots$ and the speed of light c, causing multiple blind zones in the range domain.

The knowledge on these GMTI sensor blind zones can be incorporated into a Bayesian tracking filter. This is accomplished by resembling the blind zone's influence on the detection probability [15]–[17]. First of all, notch functions are introduced which measure the distance between the target state and the blind zone center. These are in Cartesian coordinates given for the range-rate domain by

$$n_D^{\pm i}(\mathbf{x}_k, \mathbf{r}_k^S, \dot{r}_B) = \frac{\mathbf{r}_k - \mathbf{r}_k^S}{||\mathbf{r}_k - \mathbf{r}_k^S||} \dot{\mathbf{r}}_k \pm i\, \dot{r}_B\, , \;\; i = 0, 1, 2, \ldots \quad (5)$$

and for the range domain by

$$n_R^j(\mathbf{x}_k, \mathbf{r}_k^S, R_u) = ||\mathbf{r}_k - \mathbf{r}_k^S|| - j\, R_u\, , \;\; j = 1, 2, 3, \ldots \;\; , \quad (6)$$

where $\mathbf{r}_k^S$ is the sensor position vector at time step t_k. Following the argument in [15] and changing the order index of the Doppler blind zone to $l = i + 1$, the target state dependent detection probability is given by

$$\begin{aligned} P_d(\mathbf{x}_k, \mathbf{r}_k^S, \dot{r}_B, R_u) \;\; &= \;\; p_d(r_k, \varphi_k, \theta_k) \times \\ &\times \left[1 - q_D \sum_{l=1}^{\infty} e^{-\log 2 \left(\frac{n_D^{\pm l}(\mathbf{x}_k, \mathbf{r}_k^S, \dot{r}_B)}{\mathrm{MDV}} \right)^2} \right] \times \\ &\times \left[1 - q_R \sum_{j=1}^{\infty} e^{-\log 2 \left(\frac{n_R^j(\mathbf{x}_k, \mathbf{r}_k^S, R_u)}{\sigma_R} \right)^2} \right] \;\; , \end{aligned} \quad (7)$$

where the influence of the Doppler and range blind zones are modeled by Gaussian-type functions. The factors q_D and q_R are for normalization and MDV is the minimum detectable velocity of the GMTI sensor. The latter is also a measure for the width of the Doppler blind zones. The width of each range blind zone, denoted by σ_R, is determined by the pulse length τ of the chosen signal waveform and is approximately given by $\sigma_R = 2\, \tau\, c$. To retain the Gaussian framework of the tracking filter, the nonlinear notch functions $n_D^{\pm l}(\mathbf{x}_k, \mathbf{r}_k^S, \dot{r}_B)$ and $n_R^j(\mathbf{x}_k, \mathbf{r}_k^S, R_u)$ are linearized around the predicted target state $\mathbf{x}_{k|k-1}$ at time step t_k before the detection probability (7) can be substituted into the general likelihood function. The Doppler notch function is approximated by

$$n_D^{\pm l}(\mathbf{x}_k, \mathbf{r}_k^S, \dot{r}_B) \approx \tilde{z}_{D,k}^{\pm l} - \tilde{\mathbf{H}}_{D,k}^{\pm l}\, \mathbf{x}_k \quad (8)$$

with

$$\begin{aligned} \tilde{z}_{D,k}^{\pm l} \;\; &= \;\; n_D^{\pm l}(\mathbf{x}_{k|k-1}, \mathbf{r}_k^S, \dot{r}_B) + \tilde{\mathbf{H}}_{D,k}^{\pm l}\, \mathbf{x}_{k|k-1} \quad (9) \\ \tilde{\mathbf{H}}_{D,k}^{\pm l} \;\; &= \;\; -\frac{\partial}{\partial \mathbf{x}_k} n_D^{\pm l}(\mathbf{x}_k, \mathbf{r}_k^S, \dot{r}_B)\Big|_{\mathbf{x}_k = \mathbf{x}_{k|k-1}} \quad , \quad (10) \end{aligned}$$

and the range notch function is approximated by

$$n_R^j(\mathbf{x}_k, \mathbf{r}_k^S, R_u) \approx \tilde{z}_{R,k}^j - \tilde{\mathbf{H}}_{R,k}^j\, \mathbf{x}_k \quad (11)$$

with

$$\begin{aligned} \tilde{z}_{R,k}^j \;\; &= \;\; n_R^j(\mathbf{x}_{k|k-1}, \mathbf{r}_k^S, R_u) + \tilde{\mathbf{H}}_{R,k}^j\, \mathbf{x}_{k|k-1} \quad (12) \\ \tilde{\mathbf{H}}_{R,k}^j \;\; &= \;\; -\frac{\partial}{\partial \mathbf{x}_k} n_R^j(\mathbf{x}_k, \mathbf{r}_k^S, R_u)\Big|_{\mathbf{x}_k = \mathbf{x}_{k|k-1}} \quad . \quad (13) \end{aligned}$$

In that way, the exponentials in (7) can be rewritten as real Gaussians, yielding

$$\begin{aligned} P_d(\mathbf{x}_k, \mathbf{r}_k^S, \dot{r}_B, R_u) \quad &= \quad p_d(r_k, \varphi_k, \theta_k) \times \\ &\times \left[1 - q_D \sum_{l=1}^{\infty} c_D \, \mathcal{N}(\tilde{z}_{D,k}^{\pm l}; \tilde{\mathbf{H}}_{D,k}^{\pm l} \, \mathbf{x}_k, v_D) \right] \times \\ &\times \left[1 - q_R \sum_{j=1}^{\infty} c_R \, \mathcal{N}(\tilde{z}_{R,k}^{j}; \tilde{\mathbf{H}}_{R,k}^{j} \, \mathbf{x}_k, v_R) \right] \end{aligned} \quad (14)$$

with $c_D = \mathrm{MDV}/\sqrt{\log(2)/\pi}$, $v_D = \mathrm{MDV}^2/(2\log 2)$, $c_R = \frac{\sigma_R}{\sqrt{\log(2)/\pi}}$ and $v_R = \frac{\sigma_R^2}{2\log(2)}$.

2) Road Network Information: This section briefly summarizes the tracking scheme utilizing road information. More details can be found in, e.g., [1], [6].

A road is mathematically described by a continuous 3-D curve in Cartesian coordinates and is parametrized by the corresponding arc length l. This continuous curve can be approximated by a polygonal curve consisting of n_r piecewise linear segments. Each segment s with $s = 1, ..., n_r$ of the polygonal road is fully determined by the node vector $\mathbf{r}_s$, the arc length $\lambda_s = l_{s+1} - l_s$, and the normalized tangential vector $\mathbf{t}_s$. In addition, the accuracy of the road can be described by a covariance matrix $\mathbf{R}_s^r$ which also accounts for the discretization error. Details on how to compute these quantities can be found in, e.g., [1], [6], [18].

In case of targets moving on a road, it seems reasonable to describe the kinematic state vector $\mathbf{x}_k^r$ of road targets at time t_k by its position on the road l_k, i.e., the arc length of the curve, and its scalar speed $\dot{l}_k$: $\mathbf{x}_k^r = (l_k, \dot{l}_k)^\top$. By making use of the related transition density $p(\mathbf{x}_k^r|\mathbf{x}_{k-1}^r)$, the predicted density in road coordinates is given by

$$p(\mathbf{x}_k^r|\mathcal{Z}^{k-1}) = \int p(\mathbf{x}_k^r|\mathbf{x}_{k-1}^r) \, p(\mathbf{x}_{k-1}^r|\mathcal{Z}^{k-1}) \, d\mathbf{x}_{k-1}^r \, . \quad (15)$$

The problem is that the target dynamics is given in road coordinates while the measurements and, hence, the filter update is performed in Cartesian ground coordinates. In principle, the Bayesian formalism can be applied to road targets, if there exists a transformation operator $\mathcal{T}_{g \leftarrow r}$ which transforms the predicted density $p(\mathbf{x}_k^r|\mathcal{Z}^{k-1})$ from road to ground coordinates:

$$\underbrace{p(\mathbf{x}_k^r|\mathcal{Z}^{k-1})}_{\text{in road coordinates}} \quad \xrightarrow[\text{road-map error}]{\text{road-map}} \quad \underbrace{p(\mathbf{x}_k^g|\mathcal{Z}^{k-1})}_{\text{in ground coordinates}} \quad (16)$$

In general such a transformation is highly nonlinear, and the structure of probability densities in terms of Gaussian sums cannot be preserved. Linearity is, however, conserved by employing the linearized road segments for the mapping between road and ground coordinates. In this case, the density in ground coordinates, $p(\mathbf{x}_k^g|\mathcal{Z}^{k-1})$, can be written as a sum over the road segments considered:

$$p(\mathbf{x}_k^g|\mathcal{Z}^{k-1}) = \sum_{s=1}^{n_r} p(\mathbf{x}_k^g|s, \mathcal{Z}^{k-1}) \, p(s|\mathcal{Z}^{k-1}) \, . \quad (17)$$

Here, $p(s|\mathcal{Z}^{k-1})$ denotes the probability that the target moves on segment s given the accumulated sensor data $\mathcal{Z}^{k-1}$. Its explicit form is given in [6]. The densities $p(\mathbf{x}_k^g|s, \mathcal{Z}^{k-1})$ can be calculated from the probability density in road coordinates and are approximately given by Gaussians. The filtering step then recalculates the weight of each road segment and can, hence, also reweight the total road probabilities. After the filtering step, the inverse transform from Cartesian to road coordinates is simply provided by individually projecting the densities $p(\mathbf{x}_k^g|s, \mathcal{Z}^k)$ onto the associated road segments:

$$\underbrace{p(\mathbf{x}_k^g|s, \mathcal{Z}^k)}_{\text{in ground coordinates}} \quad \xrightarrow{\text{road-map}} \quad \underbrace{p(\mathbf{x}_k^r|s, \mathcal{Z}^k)}_{\text{in road coordinates}} \quad (18)$$

Before the subsequent prediction of the next iterative cycle is performed, the mixture densities are approximated by second-order moment matching [8]:

$$p(\mathbf{x}_k^r|\mathcal{Z}^k) = \sum_{s=1}^{n_r} p(s|\mathcal{Z}^k) \, p(\mathbf{x}_k^r|s, \mathcal{Z}^k) \approx \mathcal{N}\big(\mathbf{x}_k^r; \, \mathbf{x}_{k|k}^r, \, \mathbf{P}_{k|k}^r\big). \quad (19)$$

In case of a digitized road network comprised of several road sections, each section consists of a certain number of linear segments which are connected at specific nodes. This yields a complex structure exhibiting crossings and junctions. The main idea of the utilized tracking scheme with complex road-map data is to introduce a local road for each road target consisting of only a limited number of segments. Depending on the specific motion of a target along the road network, this local road is adjusted continuously.

The arising ambiguity in the vicinity of junctions and crossings is resolved over time by utilizing a multiple model approach with respect to the generated local roads: Every possible path of the moving object at the junction or crossing leads to different road hypotheses h with $h = 1, ..., N_h$, each having a different continuation of the previous local road after the junction, see Fig. 1. Whenever a target approaches a junction or crossing, a road hypothesis h for every possible continuation after the junction is generated and its probability conditioned on the accumulated sensor data, $P_k(h|\mathcal{Z}^k)$, is then calculated at the end of the filter update based on the associated road

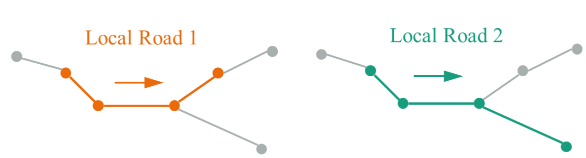

Fig. 1. Local roads generated for a target which moves from left to right and approaches the junction.

segment weights. The ambiguity is then resolved over time as the target passes the junction or crossing and moves further away so that the obtained target measurements facilitate the discrimination among the different road hypotheses. In the end, a single hypothesis will dominate and all others can be deleted.

3) Target RCS and Signal Strength Measurements: The fluctuations of the target RCS which result in fluctuations of the signal strength measurement are described by the Swerling cases [19]. In particular, RCS fluctuations according to the Swerling-I model are considered. This model assumes slow and independent fluctuations from pulse to pulse and that no fluctuations occur during a single illumination period. The signal amplitude is Rayleigh distributed. It can easily be shown [2], [3] that the pdf of the signal strength measurement a_k, conditioned on the mean signal strength ratio (SNR) at time step t_k, SNR_k, is given by

$$p(a_k|SNR_k) = \frac{1}{SNR_k} e^{-a_k/SNR_k} \quad . \tag{20}$$

The functional relationship between the instantaneous target RCS σ_k^t and mean signal strength SNR_k is determined by the radar range equation [20] which can be written as

$$SNR_k = SNR_0 \left(\frac{\sigma_k^t}{\sigma_0}\right) \left(\frac{e_k}{e_0}\right) \left(\frac{r_k}{e_0}\right)^{-4} \quad , \tag{21}$$

where SNR_0, σ_0, e_0 and r_0 are the mean SNR, RCS, illumination energy and distance of a reference target, respectively. Thus, a_k can be regarded as a measurement of the relative RCS $\sigma_k = \sigma_k^t/\sigma_0$ and with $\alpha_k = SNR_0\ (e_k/e_0)\ (r_k/e_0)^{-4}$, the relationship can simply be expressed by $SNR_k = \alpha_k \sigma_k$.

The detection probability factor p_d in (14) depends on the mean target signal strength and the detector threshold ξ. Assuming strong target returns, i.e., $1 + SNR_k \approx SNR_k$, it is given for Swerling-I fluctuations by

$$p_d^I = e^{-\xi/SNR_k} \quad . \tag{22}$$

As detections are only available if $a_k > \xi$, the signal strength measurement pdf (20) has to be normalized with the normalization factor being equal to p_d^I.

Based on this RCS fluctuation and signal strength measurement modeling, a recursive RCS update scheme can be derived for the relative RCS σ_k. This was first performed for air targets in a clutter-free environment [18] and then generalized to targets in clutter [2], [3].

C. Integrated CPHD Filter

In order to incorporate the RCS estimation scheme [2], [3], the first step is to augment the target state vector by the RCS random variable, $\mathbf{X}_k = [\mathbf{x}_k, \sigma_k]$. Likewise, the measurement set at t_k now consists of $Z_k = \{\mathbf{z}_k^m, a_k^m\}_{m=1}^{m_k}$. In addition, each component of the intensity function (1) needs to be augmented by a probability density which describes the distribution of the relative target RCS. Following the argument in [18], the class of inverse Gamma densities is chosen as

$$\mathcal{IG}(\sigma; \hat{\sigma}, \mu) = \frac{[(\mu-1)\hat{\sigma}]^{\mu}}{\Gamma(\mu)} \sigma^{-\mu-1}\, e^{-\frac{(\mu-1)\hat{\sigma}}{\sigma}} \tag{23}$$

with the expectation value $\hat{\sigma}$ and variance $\hat{\sigma}^2/(\mu-2)$. The latter only exists if $\mu > 2$.

Utilizing road network information yields an intensity function which partially consists of components processed based on an update scheme without utilizing road information and partially based on the following scheme, also accounting for digitized road network data: Without loss of generality, it is assumed that component n of the PHD surface at time step t_{k-1} is associated with a road target track related to road hypothesis h, given by

$$\begin{aligned} v_{k-1|k-1}^n(\mathbf{X}_{k-1}^r) \ &= \ w_{k-1}^n\, \mathcal{IG}(\sigma_{k-1}; \sigma_{k-1|k-1}^n, \mu_{k-1|k-1}^n) \times \\ &\quad \times \mathcal{N}(\mathbf{x}_{k-1}^r; \mathbf{x}_{k-1|k-1}^{(r)n}, \mathbf{P}_{k-1|k-1}^{(r)n}) \quad . \end{aligned} \tag{24}$$

Following the proceeding presented in Section II-B2, in the prediction step this single PHD component is decomposed into a mixture over linear road segments of the associated local road and transformed into the ground coordinate system, yielding

$$\begin{aligned} v_{k|k-1}^n(\mathbf{X}_k^g) \ &= \\ &\sum_{s=1}^{n_r(h)} P_k^h(s|n, \mathcal{Z}^{k-1})\, \mathcal{IG}(\sigma_k; \sigma_{k|k-1}^n(s), \mu_{k|k-1}^n(s)) \times \\ &\times \mathcal{N}(\mathbf{x}_k^g; \mathbf{x}_{k|k-1}^{(g)n}(s), \mathbf{P}_{k|k-1}^{(g)n}(s)) \quad . \end{aligned} \tag{25}$$

In the filter update step, each of these segment-dependent components is then used to derive $v_{k|k}^n(\mathbf{X}_k^g)$.

The processing of multiple blind zones is accomplished by making use of the generalized detection probability from Section II-B1,

$$\begin{aligned} P_d(\mathbf{X}_k^g, \mathbf{r}_k^S, \dot{r}_B, R_u) \ &= \ p_d(\mathbf{x}_k^g, \sigma_k, \mathbf{r}_k^S) \times \\ &\times \left[1 - q_D \sum_{l=1}^{\infty} c_D\, \mathcal{N}(\tilde{z}_{D,k}^{\pm l}; \tilde{\mathbf{H}}_{D,k}^{\pm l}\ \mathbf{x}_k^g, v_D)\right] \times \\ &\times \left[1 - q_R \sum_{j=1}^{\infty} c_R\, \mathcal{N}(\tilde{z}_{R,k}^{j}; \tilde{\mathbf{H}}_{R,k}^{j}\ \mathbf{x}_k^g, v_R)\right] \quad , \end{aligned} \tag{26}$$

where the prefactor $p_d(\mathbf{x}_k^g, \sigma_k, \mathbf{r}_k^S)$ is determined by the Swerling-I detection probability (22). In addition, the mean signal strength is given by $SNR_k = \alpha_k^* \sigma_k$ with

$$\alpha_k^* = SNR_0 \left(\frac{e_k}{e_0}\right) \left(\frac{r_k}{r_0}\right)^{-4} D_k^S(\varphi_k) \quad , \tag{27}$$

thus also accounting for the directivity pattern of the sensor in azimuth direction φ_k with $D_k^S(\varphi_k) = \cos(\varphi_k)^{3/2}$.

It should be pointed out that the RCS information depends on the specific road hypothesis, see (24) and (25). This is due to the fact that the filter update equations of $\sigma_{k|k}$ depend on $\alpha_k^* \sim$

$1/r_k^4$, as stated in (27), and thus implicitly on the kinematic target state. In addition, each component of the PHD generated by the blind zone hypotheses contains RCS contributions, see, e.g., (31). Thus, RCS information is also combined with blind zone knowledge within the filtering process.

Inserting the generalized probability of detection (26) into (2) then yields for the detection part

$$
\begin{aligned}
&P_d(\mathbf{X}_k^g, \mathbf{r}_k^S, \dot{r}_B, R_u)\,\frac{\mathcal{L}(Z_k|D)}{\mathcal{L}(Z_k)}\,v_{k|k-1}^n(\mathbf{X}_k^g) \;= \\
&\sum_{l=0}^{\infty}\sum_{j=0}^{\infty}\sum_{m=1}^{m_k}\sum_{s=1}^{n_r(h)} p_k^{ljmn}(s)\,\mathcal{IG}(\sigma_k;\sigma_{k|k}^{ljmn}(s),\mu_{k|k}^{ljmn}(s))\;\times \\
&\times\mathcal{N}(\mathbf{x}_k^g;\mathbf{x}_{k|k}^{(g)ljmn}(s),\mathbf{P}_{k|k}^{(g)ljmn}(s))
\end{aligned}
\tag{28}
$$

and for the missed detection part

$$
\begin{aligned}
&(1-P_d(\mathbf{X}_k^g, \mathbf{r}_k^S, \dot{r}_B, R_u))\,\frac{\mathcal{L}(Z_k|\neg D)}{\mathcal{L}(Z_k)}\,v_{k|k-1}^n(\mathbf{X}_k^g) \;= \\
&\sum_{l=0}^{\infty}\sum_{j=0}^{\infty}\sum_{s=1}^{n_r(h)} p_k^{lj0n}(s)\,\mathcal{IG}(\sigma_k;\sigma_{k|k}^{lj0n}(s),\mu_{k|k}^{lj0n}(s))\;\times \\
&\times\mathcal{N}(\mathbf{x}_k^g;\mathbf{x}_{k|k}^{(g)lj0n}(s),\mathbf{P}_{k|k}^{(g)lj0n}(s))\;.
\end{aligned}
\tag{29}
$$

The corresponding unnormalized weight factors for $m > 0$ are given by[1]

$$
\begin{aligned}
p_k^{ljmn} \;&=\; w_{k|k-1}^n\,\frac{\mathcal{L}(Z_k|m)}{\mathcal{L}(Z_k)}\;\times \\
&\times\begin{cases}
l=0,\, j=0,\, m>0: \\
\mathcal{N}(\mathbf{z}_k^m;\mathbf{H}_k\mathbf{x}_{k|k-1}^{(g)n},\mathbf{S}_k^{00m})\,\frac{\mu_{k|k-1}}{(\mu_{k|k-1}-1)\sigma_{k|k-1}}\times \\
\times\left[\frac{(\mu_{k|k-1}-1)\sigma_{k|k-1}}{(\mu_{k|k-1}-1)\sigma_{k|k-1}+a_k^m/\alpha_k^*}\right]^{\mu_{k|k-1}+1} \\[2ex]
l>0,\, j=0,\, m>0: \\
-\,q_D\,c_D\,\mathcal{N}(\tilde{z}_{D,k}^{\pm l};\tilde{\mathbf{H}}_{D,k}^{\pm l}\,\mathbf{x}_{k|k}^{(g)00m},\mathbf{S}_k^{l0m})\times \\
\times\mathcal{N}(\mathbf{z}_k^m;\mathbf{H}_k\mathbf{x}_{k|k-1}^{(g)n},\mathbf{S}_k^{00m})\times \\
\times\frac{\mu_{k|k-1}}{(\mu_{k|k-1}-1)\sigma_{k|k-1}}\left[\frac{(\mu_{k|k-1}-1)\sigma_{k|k-1}}{(\mu_{k|k-1}-1)\sigma_{k|k-1}+a_k^m/\alpha_k^*}\right]^{\mu_{k|k-1}+1} \\[2ex]
l=0,\, j>0,\, m>0: \\
-\,q_R\,c_R\,\mathcal{N}(\tilde{z}_{R,k}^{j};\tilde{\mathbf{H}}_{R,k}^{j}\,\mathbf{x}_{k|k}^{(g)00m},\mathbf{S}_k^{0jm})\times \\
\times\mathcal{N}(\mathbf{z}_k^m;\mathbf{H}_k\mathbf{x}_{k|k-1}^{(g)n},\mathbf{S}_k^{00m})\times \\
\times\frac{\mu_{k|k-1}}{(\mu_{k|k-1}-1)\sigma_{k|k-1}}\left[\frac{(\mu_{k|k-1}-1)\sigma_{k|k-1}}{(\mu_{k|k-1}-1)\sigma_{k|k-1}+a_k^m/\alpha_k^*}\right]^{\mu_{k|k-1}+1} \\[2ex]
l>0,\, j>0,\, m>0: \\
q_D\,c_D\,\mathcal{N}(\tilde{z}_{D,k}^{\pm l};\tilde{\mathbf{H}}_{D,k}^{\pm l}\,\mathbf{x}_{k|k}^{(g)0jm},\mathbf{S}_k^{ljm})\times \\
\times\,q_R\,c_R\,\mathcal{N}(\tilde{z}_{R,k}^{j};\tilde{\mathbf{H}}_{R,k}^{j}\,\mathbf{x}_{k|k}^{(g)00m},\mathbf{S}_k^{0jm})\times \\
\times\mathcal{N}(\mathbf{z}_k^m;\mathbf{H}_k\,\mathbf{x}_{k|k-1}^{(g)n},\mathbf{S}_k^{00m})\times \\
\times\frac{\mu_{k|k-1}}{(\mu_{k|k-1}-1)\sigma_{k|k-1}}\left[\frac{(\mu_{k|k-1}-1)\sigma_{k|k-1}}{(\mu_{k|k-1}-1)\sigma_{k|k-1}+a_k^m/\alpha_k^*}\right]^{\mu_{k|k-1}+1}
\end{cases}
\end{aligned}
\tag{30}
$$

[1]The road segment index s is dropped in (30) and (31) for convenience.

and for $m = 0$ determined by

$$
\begin{aligned}
p_k^{lj0n} \;&=\; w_{k|k-1}^n\,\frac{\mathcal{L}(Z_k|\neg D)}{\mathcal{L}(Z_k)}\;\times \\
&\times\begin{cases}
l=0,\, j=0,\, m=0: \\
1-\left[\sigma_{k|k-1}\Big/\left(\sigma_{k|k-1}+\frac{\xi/\alpha_k^*}{\mu_{k|k-1}-1}\right)\right]^{\mu_{k|k-1}} \\[2ex]
l>0,\, j=0,\, m=0: \\
\left[\sigma_{k|k-1}\Big/\left(\sigma_{k|k-1}+\frac{\xi/\alpha_k^*}{\mu_{k|k-1}-1}\right)\right]^{\mu_{k|k-1}}\times \\
\times\,q_D\,c_D\,\mathcal{N}(\tilde{z}_{D,k}^{\pm l};\tilde{\mathbf{H}}_{D,k}^{\pm l}\,\mathbf{x}_{k|k-1}^{(g)n},\mathbf{S}_k^{l00}) \\[2ex]
l=0,\, j>0,\, m=0: \\
\left[\sigma_{k|k-1}\Big/\left(\sigma_{k|k-1}+\frac{\xi/\alpha_k^*}{\mu_{k|k-1}-1}\right)\right]^{\mu_{k|k-1}}\times \\
\times\,q_R\,c_R\,\mathcal{N}(\tilde{z}_{R,k}^{j};\tilde{\mathbf{H}}_{R,k}^{j}\,\mathbf{x}_{k|k-1}^{(g)n},\mathbf{S}_k^{0j0}) \\[2ex]
l>0,\, j>0,\, m=0: \\
-\left[\sigma_{k|k-1}\Big/\left(\sigma_{k|k-1}+\frac{\xi/\alpha_k^*}{\mu_{k|k-1}-1}\right)\right]^{\mu_{k|k-1}}\times \\
\times\,q_D\,c_D\,\mathcal{N}(\tilde{z}_{D,k}^{\pm l};\tilde{\mathbf{H}}_{D,k}^{\pm l}\,\mathbf{x}_{k|k}^{(g)0j0},\mathbf{S}_k^{lj0})\times \\
\times\,q_R\,c_R\,\mathcal{N}(\tilde{z}_{R,k}^{j};\tilde{\mathbf{H}}_{R,k}^{j}\,\mathbf{x}_{k|k-1}^{(g)n},\mathbf{S}_k^{0j0})\;,
\end{cases}
\end{aligned}
\tag{31}
$$

where the likelihood ratios above depend on the single-target likelihood function for kinematic as well as signal strength measurements, given by

$$
L_k^m \;=\; \frac{1}{n_{k|k-1}}\int v_{k|k-1}(\mathbf{x}_k)\,p(\mathbf{z}_k^m|\mathbf{x}_k)\,p(a_k^m|\mathrm{SNR}_k)\,d\mathbf{x}_k \tag{32}
$$

$$
\begin{aligned}
&=\;\frac{1}{n_{k|k-1}}\sum_{n=1}^{N_{k|k-1}} w_{k|k-1}^n\,\mathcal{N}(\mathbf{z}_k^m;\mathbf{H}_k\,\mathbf{x}_{k|k-1}^n,\mathbf{S}_k^{mn})\;\times \\
&\quad\times\frac{\mu_{k|k-1}^n}{(\mu_{k|k-1}^n-1)\,\sigma_{k|k-1}^n}\;\times \\
&\quad\times\left[\frac{(\mu_{k|k-1}^n-1)\,\sigma_{k|k-1}^n}{(\mu_{k|k-1}^n-1)\,\sigma_{k|k-1}^n+a_k^m/\alpha_k^{*n}}\right]^{\mu_{k|k-1}^n+1}\;.
\end{aligned}
\tag{33}
$$

After evaluating all $(ljmn)$ generated components on each segment s of the associated local road, each component is then projected back onto the corresponding road segment. The moment matching technique is finally used for merging over all segments of each $(ljmn)$ index combination, yielding a mixture in continuous road coordinates as

$$
\begin{aligned}
v_{k|k}^n(\mathbf{X}_k^r) \;&=\; \sum_{l=0}^{\infty}\sum_{j=0}^{\infty}\sum_{m=0}^{m_k} w_{k|k}^{ljmn}\,\mathcal{IG}(\sigma_k;\sigma_{k|k}^{ljmn},\mu_{k|k}^{ljmn})\;\times \\
&\quad\times\mathcal{N}(\mathbf{x}_k^r;\mathbf{x}_{k|k}^{(r)ljmn},\mathbf{P}_{k|k}^{(r)ljmn})\;.
\end{aligned}
\tag{34}
$$

Regarding the weight factors, one has to make sure that if more than a single road hypothesis exists, then all PHD component weights associated with either road hypothesis have to be divided by the total number of road hypotheses. This guarantees that the sum of weights still yields the estimated number of targets.

III. Performance Evaluation

The performance evaluation focuses on a scenario setup with two ground targets moving along a simple road network layout. The trajectories of the two targets and the airborne monostatic GMTI radar platform are shown in Fig. 2. The paths of the targets can be divided into three sections: During the first part, the two targets are spatially separated most of the time. In the second part, both targets move closely-spaced along the same trajectory for a considerable period of time, performing a simultaneous move-stop-move maneuver with a stopping period of 20 s. And in the third part, the targets finally move apart from each other again. The chosen scenario and tracking parameters are listed in Tab. I.

The main challenges of this specific scenario become obvious by looking at Fig. 3. The left plot shows the evolution of the corresponding range-rates of the two targets and the main lobe clutter and also indicates the locations of the multiple Doppler blind zones. Due to the move-stop-move maneuver of both targets, the range-rate values drop into the blind zone region quickly and remain at the blind zone's center until the target radial velocities again exceed the MDV of the sensor system. The right plot shows the evolution of the slant range for the corresponding positions of the two targets on the ground w.r.t. the airborne GMTI radar and the location of the blind zones in the range domain. Both targets are affected by the same range blind zone, shortly before they move apart from each other in the final part of the scenario. Thus, the challenges a tracking filter has to face can be summarized as follows: As soon as the two targets move closely-spaced along the same road segment, the track identity, i.e., the correct target-track association will be lost if only kinematic sensor information is exploited. And as both targets exhibit roughly the same kinematic state vector during this part of the scenario, it is likely that the PHD components of the utilized CPHD filter, associated with the two targets, are quickly merged, so that a single component with weight close to 2 substitutes the previous two single PHD components, each with weight factors close to 1. The tracking filter also has to deal with the long sequence of unobservability caused by the simultaneous stop of the two targets and the resulting masking by the Doppler blind zone of the sensor. The range blind zone finally poses an additional challenge for the employed tracking filter.

As multiple closely-spaced targets are present, this scenario was analyzed based on different variants of the CPHD filter. Due to the possible three classes of information to be incorporated into the tracking algorithm, a total of eight different CPHD filter variants were considered in this analysis. In order to assess the performance of each filter, the following measures of performance were studied: a) the track continuity, i.e., the capability of the filter to maintain a once extracted track for each target until the final revisit, b) the probability of the correct target-track association at the final revisit and c) the mean optimal subpattern assignment (OSPA) value based on a modified version of the OSPA metric with labeling errors [3]. The obtained simulation results based on 100 Monte Carlo runs are listed in Tab. II. Exemplary multi-target tracking results for each CPHD filter variant are presented in Fig. 4. For the calculation of the OSPA value at each revisit, the maximum cardinality penalty was set to $500\,\mathrm{m}$ and the corresponding penalty for labeling errors was set to $250\,\mathrm{m}$.

The standard CPHD filter reached a track continuity of zero, i.e., it was not able to maintain the two tracks until the final revisit in any Monte Carlo run. The exemplary tracking performance, shown in the corresponding plot of Fig. 4, reveals

TABLE I
Simulation Parameters

Total number of revisits	N	=	225
Revisit time	ΔT	=	1 s
Ground target speed	v_t	=	$20\,\mathrm{m/s}$
Sensor velocity	v_p	=	$[90, 0, 0]\,\mathrm{m/s}$
Sensor altitude	z_p	=	$3\,\mathrm{km}$
Range standard deviation	σ_r	=	$10\,\mathrm{m}$
Azimuth standard deviation	σ_φ	=	$0.5°$
Elevation standard deviation	σ_θ	=	$0.5°$
Range-rate standard deviation	$\sigma_{\dot{r}}$	=	$0.01\,\mathrm{m/s}$
Mean false alarm rate	$\bar{n}_{fa}$	=	1/FoV/Scan
False alarm probability	P_{fa}	=	10^{-2}
Mean RCS values	σ_{t_1/t_2}	=	$[1; 4]\,\mathrm{m}^2$
RCS of reference target	σ_0	=	$1\,\mathrm{m}^2$
Slant range of reference target	r_0	=	$24\,\mathrm{km}$
SNR of reference target	SNR_0	=	13 dB
Mean SNR of false alarm	CNR	=	10 dB
Pulse-Doppler radar PRF	f_{PRF}	=	8700 Hz
Pulse-Doppler radar pulse width	τ	=	$0.45 \times 10^{-6}\,\mathrm{s}$
Motion model process noise	σ_p	=	$2.5\,\mathrm{m/s}^2$
Weight of birth component	w_{birth}	=	0.001
Survival probability	P_s	=	0.99

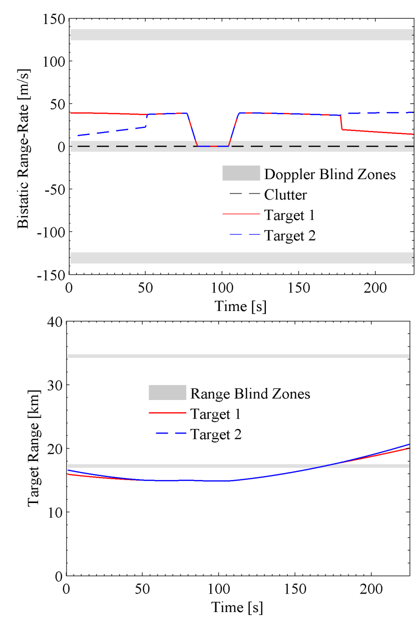

Fig. 3. Up: Evolution of the platform motion compensated bistatic range-rate of targets and main lobe clutter. The gray bands indicate the Doppler blind zones of order -1, 0 and $+1$ in the range-rate domain at each time step. Bottom: Evolution of the slant range for the corresponding positions of the two targets w.r.t. the airborne GMTI radar. The gray bands indicate the first and second blind zones in the range domain at each time step.

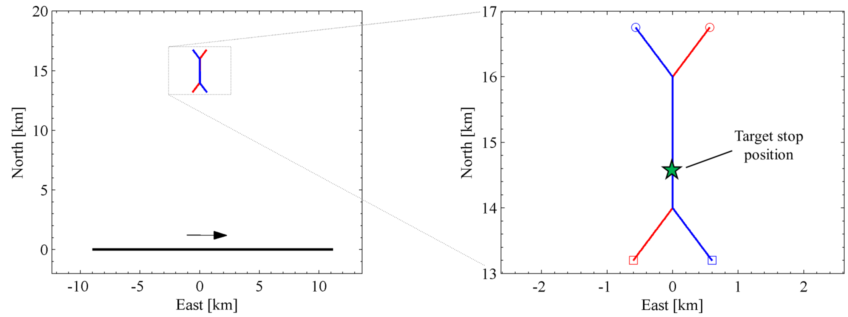

Fig. 2. Left: Scenario setup with trajectories of the two ground targets (red, blue) and of the monostatic GMTI radar platform (black). Right: Close-up view of the target trajectories along the road network. Symbols □ and ○ refer to the initial and final target positions, respectively.

that as soon as both targets started moving along the same road segment, the two tracks were merged due to the strong similarity of the two PHD components associated with each target and the missing capability to discriminate both targets based on attribute information, i.e., the mean RCS. After that, also the survived track (red) was terminated due to the long sequence of missed detections caused by the target stops. As soon as new measurements became available, a new track (green) was extracted which then described both targets, i.e., with a corresponding weight factor of 2. After the separation of the two targets, the single track followed one branch and only at for the last couple of revisits, the standard CPHD filter was able to extract another track (purple), representing the second target, so that the PHD component weights of each track were finally again roughly 1.

The CPHD variants incorporating one particular source of information reached a slightly better performance: If only the knowledge on the Doppler and range blind zones was exploited, the corresponding tracking filter (CPHD + DRBZ) was able to maintain at least one of the two tracks until the final revisit. As in the case of the standard CPHD filter, the second track was merged as soon as the statistical distance between both tracks became small enough. The second track was represented by an additional track only during the last revisits of the scenario. The CPHD variant exploiting road network information (CPHD + Road) suffered from almost the same difficulties as the standard CPHD filter with the only differences that the extracted tracks were located on the road segments for most of the time and that in this case an individual track could not be extracted as representation of the second target during the final section of the scenario in many Monte Carlo runs. Finally, the tracking filter utilizing signal strength information (CPHD + RCS) was able to discriminate the two tracks in the first half of the scenario, but suffered from track terminations due to the lacking capability of handling missed detection sequences caused by blind zone masking. Comparing these three single-information filters, the best performance in terms of the lowest mean OSPA value was achieved by the CPHD filter variant exploiting blind zone information, because this knowledge helped maintaining at least one track until the final revisit so that the overall cardinality error was smaller compared to the other two variants. Nevertheless, no CPHD filter exploiting only a single source of information was able to maintain both tracks in any Monte Carlo run, yielding a track continuity of zero for all three tracking filters. The CPHD

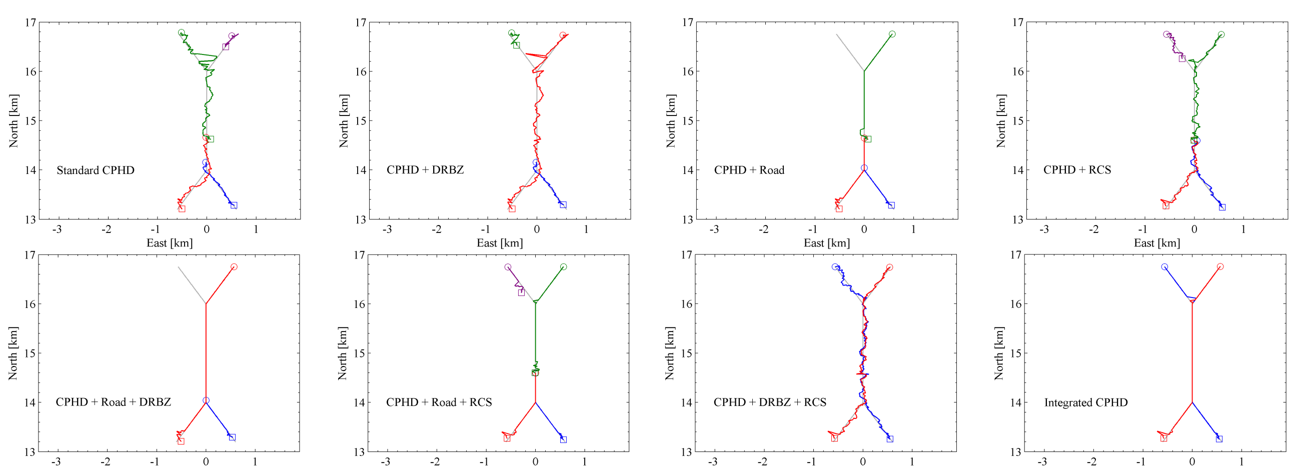

Fig. 4. Exemplary multi-target tracking results of the different CPHD filter variants based on monostatic GMTI measurements for a single Monte Carlo run. Symbols □ and ○ refer to locations of track extraction and deletion, respectively. Positions at final time instance are also indicated by ○.

TABLE II
SIMULATION RESULTS OF THE MULTI-TARGET SCENARIO BASED ON 100 MONTE CARLO RUNS FOR DIFFERENT CPHD FILTER VARIANTS.

CPHD Filter Variant	*Doppler & Range Blind Zones*	*Road Network Information*	*Signal Strength Measurements*	*Track Continuity*	*Correct Association Probability*	*Mean OSPA*
Standard CPHD	–	–	–	0 %	–	308.6 m
CPHD + DRBZ	✓	–	–	0 %	–	234.7 m
CPHD + Road	–	✓	–	0 %	–	299.8 m
CPHD + RCS	–	–	✓	0 %	–	307.7 m
CPHD + DRBZ + Road	✓	✓	–	0 %	–	243.8 m
CPHD + DRBZ + RCS	✓	–	✓	96 %	$(100 \pm 0)\%$	122.1 m
CPHD + Road + RCS	–	✓	✓	0 %	–	282.7 m
Integrated CPHD	✓	✓	✓	95 %	$(99 \pm 1)\%$	76.4 m

filter variants exploiting two sources of information reached a mixed performance compared to the previous CPHD filters: By incorporating both road and blind zone information (CPHD + Road + DRBZ), a single track could be maintained throughout the scenario with the other track being merged with the first one as soon as both tracks moved closely-spaced. But in many Monte Carlo runs, the surviving track represented both targets until the end of the scenario, thus without extracting another track for the second target as soon as both targets moved apart again. With signal strength instead of blind zone information, the resulting CPHD filter variant (CPHD + Road + RCS) yielded the same performance as the filter without exploiting road network information, with the only major difference of more precise tracks, leading to a slightly lower mean OSPA value in comparison. But the only tracking filter which was able to maintain both tracks throughout the scenario in most Monte Carlo runs (96 %), based on exploiting two sources of information, was the tracking filter CPHD + DRBZ + RCS. Incorporating both blind zone as well as signal strength information yielded a correct association probability of 100 %. The integrated CPHD filter variant finally reached the best overall performance of all examined filters by further improving the results of the tracking filter exploiting blind zone and signal strength information (CPHD + DRBZ + RCS) in terms of track precision due to the additionally exploited road network information. This yielded the lowest mean OSPA value of 76.4 m.

IV. CONCLUSION

In this paper, the standard CPHD filter was augmented by extended blind zone knowledge, road network information and signal strength measurement processing to overcome the imminent performance degradation due to the general challenges in the ground target tracking domain. Based on a systematic analysis of a challenging multi-target scenario comprising stopping and closely-spaced targets, it was demonstrated that a sophisticated combination of the chosen complementary sources of information delivered the best tracking performance in terms of track precision, track stability and track identity compared to standard or less augmented CPHD filter variants.

REFERENCES

[1] M. Mertens, M. Feldmann, M. Ulmke, and W. Koch, *Tracking and Data Fusion for Ground Surveillance*. Chapter 6 in: M. Mallick, V. Krishnamurthy, and B.-N. Vo (Eds.), Integrated Tracking, Classification, and Sensor Management: Theory and Applications, IEEE, John Wiley & Sons, 2012.

[2] M. Mertens and M. Ulmke, "Ground Moving Target Tracking Using Signal Strength Measurements with the GM-CPHD Filter," in *Proc. of the 7th Workshop Sensor Data Fusion: Trends, Solutions, Applications*, Bonn, 2012.

[3] M. Mertens and M. Ulmke, "Ground Target Tracking with RCS Estimation Utilizing Probability Hypothesis Density Filters," in *Proc. of the 16th International Conference on Information Fusion*, Istanbul, 2013.

[4] M. Mertens, T. Kirubarajan, and W. Koch, "Doppler Blind Zone Analysis for Ground Target Tracking with Bistatic Airborne GMTI Radar," in *Proc. of the 15th International Conference on Information Fusion*, Singapore, 2012.

[5] M. Mertens, T. Kirubarajan, and W. Koch, "Exploiting Doppler Blind Zone Information for Ground Moving Target Tracking with Bistatic Airborne Radar," *IEEE Transactions on Aerospace and Electronic Systems*, vol. 50(1), pp. 130 – 148, 2014.

[6] M. Ulmke and W. Koch, "Road-Map Assisted Ground Moving Target Tracking," *IEEE Transactions on Aerospace and Electronic Systems*, vol. 42(4), pp. 1264 – 1274, 2006.

[7] R. Mahler, "PHD Filters of Higher Order in Target Number," *IEEE Transactions on Aerospace and Electronic Systems*, vol. 43(4), pp. 1523 – 1543, 2007.

[8] Y. Bar-Shalom, X.-R. Li, and T. Kirubarajan, *Estimation with Applications to Tracking and Navigation: Theory, Algorithms and Software*. John Wiley & Sons, 2001.

[9] R. Mahler, *Statistical Multisource-Multitarget Information Fusion*. Artech House, 2007.

[10] B.-T. Vo, B.-N. Vo, and A. Cantoni, "Analytic Implementations of the Cardinalized Probability Hypothesis Density Filter," *IEEE Transactions on Signal Processing*, vol. 55(7), pp. 3553 – 3567, 2007.

[11] M. Ulmke, O. Erdinc, and P. Willett, "GMTI Tracking via the Gaussian Mixture Cardinalized Probability Hypothesis Density Filter," *IEEE Transactions on Aerospace and Electronic Systems*, vol. 46(4), pp. 1821 – 1833, 2010.

[12] O. Erdinc, P. Willett, and Y. Bar-Shalom, "The Bin-Occupancy Filter and Its Connection to the PHD Filters," *IEEE Transactions on Signal Processing*, vol. 57(11), pp. 4232 – 4246, 2009.

[13] J. R. Guerci, *Space-Time Adaptive Processing for Radar*. Artech House, Boston, London, 2003.

[14] R. Klemm, *Principles of Space-Time Adaptive Processing*. 3rd Edition, IET Radar, Sonar and Navigation, Series 21, 2006.

[15] W. Koch and R. Klemm, "Ground Target Tracking with STAP Radar," *IEE Proceedings - Radar, Sonar and Navigation*, vol. 148(3), pp. 173 – 185, 2001.

[16] W. Koch, "On Exploiting 'Negative' Sensor Evidence for Target Tracking and Sensor Data Fusion," in *Proc. 10th International Conference on Information Fusion*, Quebec, Canada, 2007.

[17] M. Mertens and U. Nickel, "GMTI Tracking in the Presence of Doppler and Range Ambiguities," in *Proc. of the 14th International Conference on Information Fusion*, Chicago, 2011.

[18] W. Koch, "Tracking and Data Fusion Applications," *Advanced Radar Signal and Data Processing*, Educational Notes RTO-EN-SET-086, Paper 9, France, 2006.

[19] P. Swerling, "Probability of Detection for Fluctuating Targets," *IRE Transactions on Information Theory*, vol. 6, pp. 269–308, 1960.

[20] M. Skolnik, *Radar Handbook*. Third edition, McGraw-Hill, 2008.